EGO-MOTION ESTIMATION FOR LOW-COST FREEHAND ULTRASOUND SCANNER

Ayusha Abbas *Jeffrey Neasham* *Syed Mohsen Naqvi*

Intelligent Sensing and Communications Research Group,
Newcastle University, Newcastle upon Tyne, NE1 7RU, U.K.

ABSTRACT

This paper describes work towards a very low-cost medical ultrasound imaging system using concepts of ego-motion estimation. This will enable a B-mode image to be constructed from a very simple probe with a single fixed beam which is either manually scanned across the skin (linear) or rotated against the skin (polar). In the case of a linear scan, an algorithm has been proposed which measures the decorrelation between successive scanlines to estimate probe velocity. With the aid of an Unscented Kalman Filter (UKF), this is used to reconstruct a geometrically correct 2D image of a resolution phantom which has well-defined image patterns for precise measurement of geometric accuracy. In the case of a polar scan, angular data obtained from a low cost MEMS gyroscope is used to reconstruct the image. Examples are also shown of data collected on human subjects, which show promising results for clinical diagnostics.

Index Terms**—** Egomotion estimation, Decorrelation Measurements, Mean of Absolute differences, Unscented Kalman Filter.

1. INTRODUCTION

Every day and every minute, a woman dies due to complications during pregnancy or childbirth [1]. Approximately 303,000 deaths, related to childbirth, have been recorded in 2015, of which 99% occurred in developing countries [2]. Reducing preventable maternal mortality crucially depends on ensuring that women have access to basic health care services; before, during and after childbirth [2]. Maternal mortality risk factors could be detected by using ultrasound imaging, but these devices are very expensive hence not affordable for healthcare providers in developing countries.

Conventional ultrasound devices use multi-element piezoelectric transducer array to produce a 2D or a 3D image, while only a single piezoelectric element transducer has been used in the proposed scanner. This probe design greatly reduces the hardware complexity, power consumption and beamforming computational load, hence bringing the manufacturing cost down to less than $100. This will make the device affordable to the developing countries. The block diagram for the prototype ultrasound probe and an image of an acoustic phantom being scanned with this probe could be seen in Fig.1.

Concepts of ego-motion estimation have been used to construct a B-mode image from a series of scan lines (echo data). In the most reported work [3–6] on transducer motion estimation, correlation-based techniques have been used to track transformation between successive 2D images to create a 3D image. This is done by decomposing the image into several numbers of blocks and finding the best match between a block from the first and the successive image. This is found by calculating the correlation coefficient which will describe the motion vector between those blocks.

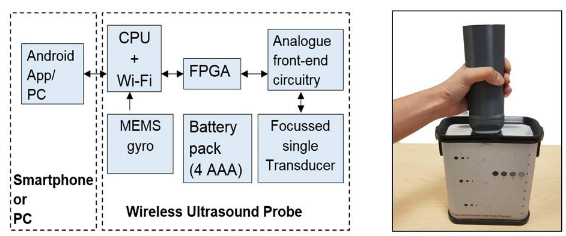

Fig. 1. (Left) Block diagram for ultrasound scanner. (Right) Set-up for scanning the phantom using this scanner.

This paper introduces a different approach for using the decorrelation technique on a series of scan lines (1D data), rather than on a 2D image. Data was obtained by either translating the probe linearly, while keeping the orientation near constant, or by only rotating the probe from the minimum to a maximum angle with no translation. Mean of absolute differences (MAD) between scanlines was found, which gives information about the velocity of the probe in a linear scan. This helps in mapping the image into a set of pixels which are geometrically correct. In the polar scan, orientation data from a MEMS gyro are used to transform the polar coordinates into the Cartesian coordinates. These coordinates allow a 2D image to be created from a series of scanlines.

These techniques have been used in previously collected human data, for *in-vivo* validation, by employing the single piezoelectric element transducer. It's bandwidth and centre frequency is 2 MHz and 4 MHz respectively. It has a focused beam optimised for 4-15 cm penetration depth and a maximum lateral resolution of 0.2 mm at the focal depth of 5 cm.

Some of the concepts used to minimise hardware complexity in the prototype probe can be seen in previous work done by our research team [7].

2. THEORY AND METHODS

2.1. Ultrasound Decorrelation Measurements

There are two motions which could be associated with an ultrasound image sequence; the motion of the transducer or the tissue which is being scanned. In experiments on a phantom, the targets will be static, which implies that the change occurring in the data will be due to the motion of the transducer. Ego-motion estimation techniques will be used to estimate the transducer's motion relative to a static scene inside the body (phantom). This will make sure that the echo data can be projected onto a set of pixels which are geometrically correct. Decorrelation measurements have been obtained by calculating the mean of absolute differences values (MAD) between consecutive scanlines. This is done through the following steps:

I. The absolute differences between the echo signal intensities of each consecutive scanlines and for all the available samples of those scanlines were calculated.

II. Mean of the absolute differences values was calculated.

III. Steps I and II were repeated for all the other scanlines by moving successively through all the data.

$$MAD = E[|x_n - x_{n-1}|] \tag{1}$$

where, x(n) and x(n-1) represent the value of echo signal intensities for consecutive scanlines at a fixed depth.

2.1.1. Velocity calculation for the ultrasound probe

Velocity was calculated after normalising the MAD values using the formula given below:

$$MAD_{norm} = \frac{\frac{1}{N}\sum(x_n - x_{n-1})}{\frac{1}{2N}\left(\sum x_n + \sum x_{n-1}\right)} \tag{2}$$

where, N represents number of samples,
$\frac{1}{N}\sum(x(n) - x(n-1)$ is the mean of absolute difference and MAD_{norm} are the normalised MAD. These values are directly proportional to the velocity of the probe.
Distance covered by the probe from one end of the phantom to the other end was calculated by integrating MAD values for one curve. This was compared with the estimated distance to find the constant of proportionality, k for this particular transducer geometry. Value of k was calibrated by looking at the final 2D image of the phantom and comparing it with the real image of the phantom. This constant was used to calculate the estimated velocity of the probe:

$$V_{estimate} = \frac{MAD_{norm}}{k} \tag{3}$$

where, $V_{estimate}$ represents the estimated velocity of probe.

2.2. Unscented Kalman filter

Unscented Kalman Filter is used to estimate the state of a non-linear system, which is the velocity of the probe.

$$Y_t = F(y_{t-1}, v_t) \tag{4}$$

$$z_t = H(y_t, w_t) \tag{5}$$

where Y_t represents the unobserved state of the system, which is the velocity of the probe and z_t is the observed state, which includes the current distance covered by the probe and velocity calculated through decorrelation techniques. v_t is the process noise and w_t is the observation noise. Unscented transformation (UT) method was used to calculate the statistics of a random variable y (dimension L) which undergoes a nonlinear transformation. A matrix $'Y'$ was formed of $2L + 1$ sigma vectors (Y_i) with corresponding weights W_i using the following equations [8]:

$$Y_0 = \mu \tag{6}$$

$$Y_i = \mu + (\sqrt{(L+\lambda)P_y})_i \qquad i = 1, ..., L \tag{7}$$

$$Y_i = \mu - (\sqrt{(L+\lambda)P_y})_{i-L} \qquad i = L+1, ..., 2L \tag{8}$$

$$W_0^m = \frac{\lambda}{(L+\lambda)} \tag{9}$$

$$W_0^c = \frac{\lambda}{(L+\lambda)} + (1 - \alpha^2 + \beta) \tag{10}$$

$$W_i^m = W_i^c = \frac{1}{\{2(L+\lambda)\}} \qquad i = 1, ..., 2L \tag{11}$$

where, λ = α^2(L+κ)-L is a scaling factor which is set to 0.1, (kappa) κ and β are set to 0 and 2 respectively. λ shows the spread of sigma point across the mean.
These sigma vectors (Y_i) become the input of the nonlinear function, $Y_t = F(y)$. Mean of weighted sample and covariance of posterior sigma points were used to approximate predicted mean and covariance [8].

$$\mu' \approx \sum_{i=0}^{2L} W_i^m F(Y_i) \tag{12}$$

$$P_y{}' \approx \sum_{i=0}^{2L} W_i^c \{F(Y_i) - \mu'\}\{F(Y_i) - \mu'\}^T \tag{13}$$

Kalman gain was calculated after the prediction step in order to update the state and covariance values. Unscented Kalman

Filter has been used to estimate/track probe velocity and our techniques [9–12] can also be investigated for non-Gaussian situations in future work.

2.3. Phantom

Data has been obtained by scanning the probe over the Precision Multi-Purpose Grey Scale Phantom, which is used to provide a way for monitoring the image quality of an ultrasound scanning system. A tissue mimicking gel has been used which is ultrasonically similar to human tissue to ensure that the measured performance will be closely approximated to the scanner's performance in the clinical examination. Grey-scale targets are provided for monitoring the contrast and temporal resolution, and distinguishing between different intensities of brightness as shown in Fig.3 [13].

2.4. Polar scan

Scan-line data was also obtained in a free-hand "polar"scan of the phantom by rotating the probe against the phantom surface about the axis of the transducer. Series of scan lines in polar coordinates are then converted to Cartesian coordinates (x,y) using this orientation data enabling them to be displayed in a B-mode ultrasound image.

3. RESULTS AND DISCUSSION

Fig.2 illustrates the relationship between estimated velocity of the probe (calculated from MAD values) and pattern of the image created from echo data, which was obtained after linearly scanning the phantom. The pulse repetition frequency is 400 Hz meaning each scan line is spaced by 2.5 ms in time and scans are performed in a period of between 0.5 and 1 second.

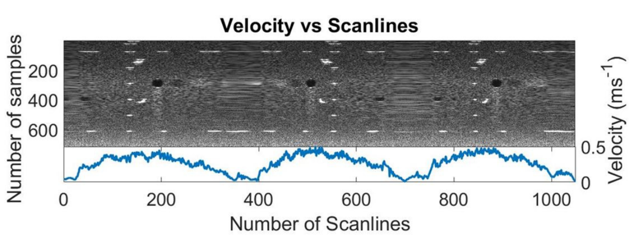

Fig. 2. Relationship between scanlines data and velocity values.

The velocity changing from the minimum to a maximum value and then returning back to the minimum value demonstrates that the probe would have moved with a low velocity at the start of the scan, high velocity in the middle and a low velocity at the end. The start and end of a scan could be found from the velocity trend, where one whole velocity curve represents a scan in one direction as shown in Fig.2.

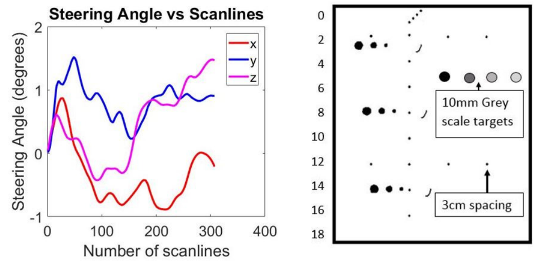

Fig. 3. (Left) Steering angles of probe for a linear scan in all three directions. (Right) Target specifications of the phantom.

Steering angles for the probe of a linear scan, in all three axes(x,y,z), could be seen in Fig.3 (left). Maximum change in angle, in either direction, is less than 2 degrees - which makes this data suitable for application of the ego-motion estimation algorithm.

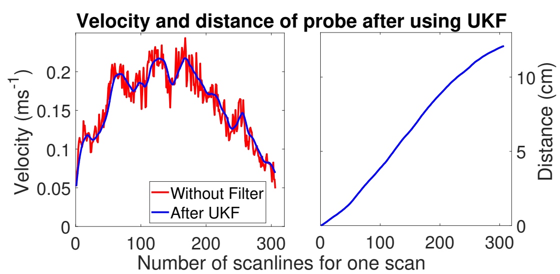

Fig. 4. (Left) Estimation of Probe's velocity. (Right) Estimation of horizontal distance covered by probe.

Unscented Kalman filter (UKF) is used to estimate the state of this non-linear system, which calculates the optimised value for the velocity and the distance of the probe as seen in Fig.4. This gives the estimated distance travelled by the probe which is used to create the geometrically correct image of the phantom.

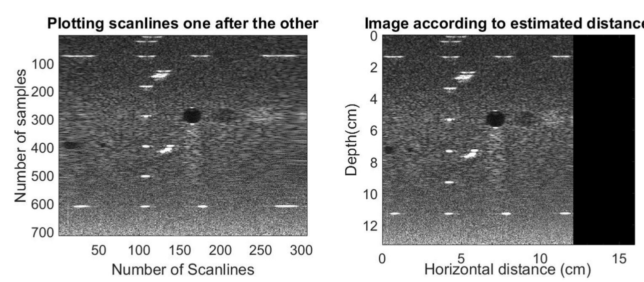

Fig. 5. (Left) Image without the use of decorrelation techniques. (Right) B-mode image after applying decorrelation techniques.

Fig.5 (left) shows a linear scan image of the phantom without the use of egomotion estimation techniques and geometry of this image could be compared with Fig.3 (right). The spacing between vertical and horizontal pin targets are not equal and the image is highly distorted at the start and the end. After applying the egomotion estimation approach, the horizontal target pins have become spaced by approximately 3cm as shown in Fig.5 (right). The image has become geometrically correct with respect to real distance of 12cm which was moved by the probe. Circular anechoic target is measured to be approximately equal to 10 mm and other greyscale targets have also started to appear more circular. Vertical pin targets are the narrowest in the focal zone because pin width demonstrates the width of the ultrasound beam at that depth and approximates the lateral resolution of the scanner. The lateral resolution of the scanner is highest at the depth of around 7cm due to the focal parameters of the transducer.

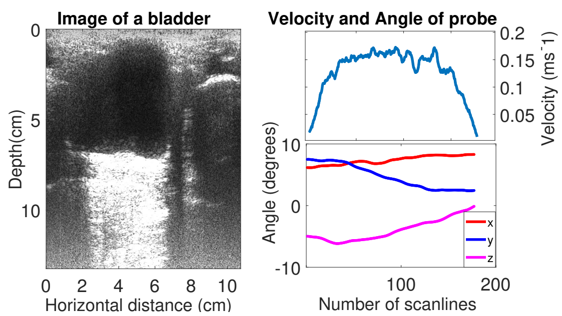

Fig. 6. (Left) Image of a bladder using decorrelation technique. (Top-Right) Estimation of velocity of the probe. (Bottom-right) Steering angles for the probe in all directions.

Decorrelation technique was tested on previously available *in-vivo* data obtained by single element piezoelectric transducer, to show that this approach could be used in real (human) data which is seen in Fig. 6 (left). For this linear scan of a bladder, velocity changes from a minimum value to maximum and then returns back to a minimum value for a complete scan. Steering angles were kept to a very minimal change during the linear scan as shown in Fig 6 (bottom right).

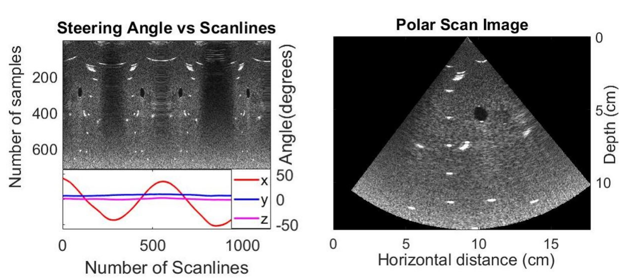

Fig. 7. (Left) Change of Steering angles with number of scanlines. (Right) Polar scan image of the phantom.

Change of steering angle from a minimum value to the maximum, depicts the completion of a polar scan as shown in Fig.7 (left). As the probe was rotated along one axis (x), angular change in the other axes is almost zero. A polar image was created in Fig.7 (right) by converting the polar coordinates into Cartesian coordinates by using these angles of x-axis. Polar scan image of a human bladder could be seen in Fig.8 which shows the possibility of using this technique in real data.

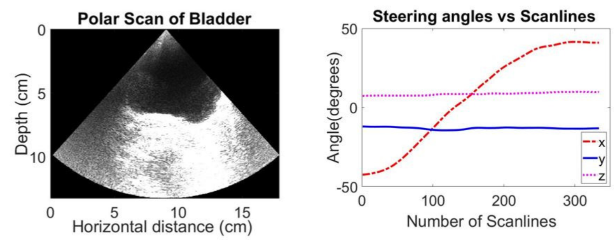

Fig. 8. (Left) Polar scan image of a human bladder. (Right) Change of steering angle with scanlines.

4. CONCLUSION AND FUTURE WORK

The production cost of the very low-cost medical ultrasound imaging system was reduced by replacing a multi-element piezoelectric transducer array with a single piezoelectric element. Raw echo data was gathered by manually scanning the transducer over the phantom or the skin, and motion data was collected from MEMS gyroscope. This data was transmitted to the computer via Wi-Fi for further processing. Ego-motion estimation algorithm has been used for processing 1D, raw echo-data to generate a 2D ultrasound image. The velocity of the probe has been estimated using decorrelation measurements and Unscented Kalman Filter. These are used to create the geometrically correct image of the phantom which is compared with the real image. The decorrelation technique is dependent on the texture or speckle detail of tissue and the focal parameters of the transducer. Hence further work is needed to optimise this algorithm to be robust in more complex scenes and variable tissue properties in human scans. Estimated values for motion will be compared with the controlled motion by using a mechanical rig in the future work.

Angular data gathered from the gyroscope was used to create a polar image by converting the polar coordinates into Cartesian coordinates. Linear and polar scan data has been processed separately with different techniques in this paper. Future work is also required to enable the algorithms to work in the case of combined motions (translation and rotation) by using the decorrelation and motion sensor data together. Initial *in-vivo* experiments have shown promising results for clinical diagnostic and with further work this technique has potential to deliver a very low cost ultrasound probe design for use in the developing world.

5. REFERENCES

[1] UNICEF, "Every day,every minute,a woman dies giving birth," https://www.unicef.org/newsline/02pr07iwd.htm, online: accessed October 2018.

[2] World Health Organization, "World health statistics 2018," http://apps.who.int/iris/bitstream/handle/10665/272596/9789241565585-eng.pdf?ua=1, online: accessed October 2018.

[3] Kevin Owen, F William Mauldin, and John A Hossack, "Transducer motion estimation using combined ultrasound signal decorrelation and optical sensor data for low-cost ultrasound systems with increased field of view," in *Ultrasonics Symposium (IUS), 2011 IEEE International*. IEEE, 2011, pp. 1431–1434.

[4] Wendy Smith and Aaron Fenster, "Statistical analysis of decorrelation-based transducer tracking for three-dimensional ultrasound," *Medical physics*, vol. 30, no. 7, pp. 1580–1591, 2003.

[5] Jian-Feng Chen, J Brian Fowlkes, Paul L Carson, and Jonathan M Rubin, "Determination of scan-plane motion using speckle decorrelation: Theoretical considerations and initial test," *International Journal of Imaging Systems and Technology*, vol. 8, no. 1, pp. 38–44, 1997.

[6] Yazan Awwad, *Motion Estimation and Registration of B-Mode Ultrasound Images for Improved Visualisation*, Ph.D. thesis, Carleton University, 2014.

[7] Thomas LA van den Heuvel, David J Graham, Kristopher J Smith, Chris L de Korte, and Jeffrey A Neasham, "Development of a low-cost medical ultrasound scanner using a monostatic synthetic aperture," *IEEE transactions on biomedical circuits and systems*, vol. 11, no. 4, pp. 849–857, 2017.

[8] Eric A Wan and Rudolph Van Der Merwe, "The unscented kalman filter for nonlinear estimation," in *Adaptive Systems for Signal Processing, Communications, and Control Symposium 2000. AS-SPCC. The IEEE 2000*. Ieee, 2000, pp. 153–158.

[9] Qian Li, Yueyang Ben, Syed Mohsen Naqvi, Jeffrey A Neasham, and Jonathon A Chambers, "Robust student's t-based cooperative navigation for autonomous underwater vehicles," *IEEE Transactions on Instrumentation and Measurement*, 2018.

[10] Pengming Feng, Wenwu Wang, Syed Mohsen Naqvi, and Jonathon Chambers, "Adaptive retrodiction particle phd filter for multiple human tracking," *IEEE Signal Processing Letters*, vol. 23, no. 11, pp. 1592–1596, 2016.

[11] Pengming Feng, Wenwu Wang, Satnam Dlay, Syed Mohsen Naqvi, and Jonathon Chambers, "Social force model-based mcmc-ocsvm particle phd filter for multiple human tracking," *IEEE Transactions on Multimedia*, vol. 19, no. 4, pp. 725–739, 2017.

[12] Syed Mohsen Naqvi Ata-ur Rehman, Lyudmila Mihaylova, and Jonathon Chambers, "Multi-target tracking and occlusion handling with learned variational bayesian clusters and a social force model," *IEEE Trans. Signal Process*, vol. 64, no. 5, pp. 1320–1335, 2016.

[13] Gammex, "403 gsle precision multi-purpose phantom8," https://www.sunnuclear.com/solutions/diagnostic/ultrasoundqa, online: accessed October 2018.